Biosensors and Bioelectronics 68 (2015) 245–252

Contents lists available at ScienceDirect

Biosensors and Bioelectronics

journal homepage: www.elsevier.com/locate/bios

Portable oxidative stress sensor: Dynamic and non-invasive measurements of extracellular H_2O_2 released by algae

Volodymyr B. Koman [a], Christian Santschi [a,*], Nadia R. von Moos [b], Vera I. Slaveykova [b], Olivier J.F. Martin [a]

[a] Nanophotonics and Metrology Laboratory (NAM), Swiss Federal Institute of Technology (EPFL), 1015 Lausanne, Switzerland
[b] Environmental Biogeochemistry and Ecotoxicology, Institute F.-A. Forel, Earth and Environmental Sciences, Faculty of Sciences, University of Geneva, 10, route de Suisse, 1290 Versoix, Switzerland

ARTICLE INFO

Article history:
Received 22 October 2014
Received in revised form
17 December 2014
Accepted 20 December 2014
Available online 23 December 2014

Keywords:
Optical detection
Multiscattering
Cytochrome *c*
Hydrogen peroxide
Toxicity

ABSTRACT

Reactive oxygen species (ROS) generated by aerobic organisms are essential for physiological processes such as cell signaling, apoptosis, immune defense and oxidative stress mechanisms. Unbalanced oxidant/antioxidant budgets are involved in many diseases and, therefore, the sensitive measurement of ROS is of great interest. Here, we present a new device for the real-time monitoring of oxidative stress by measuring one of the most stable ROS, namely hydrogen peroxide (H_2O_2). This portable oxidative stress sensor contains the heme protein cytochrome *c* (cyt *c*) as sensing element whose spectral response enables the detection of H_2O_2 down to a detection limit of 40 nM. This low detection limit is achieved by introducing cyt *c* in a random medium, enabling multiscattering that enhances the optical trajectory through the cyt *c* spot. A contact microspotting technique is used to produce reproducible and reusable cyt *c* spots which are stable for several days. Experiments in static and microfluidic regimes, as well as numerical simulations demonstrate the suitability of the cyt *c*/H_2O_2 reaction system for the real-time sensing of the kinetics of biological processes without H_2O_2 depletion in the measurement chamber. As an example, we detect the release of H_2O_2 from the green alga *Chlamydomonas reinhardtii* exposed to either 180 nM functionalized CdSe/ZnS core shell quantum dots, or to 10 mg/l TiO_2 nanoparticles. The continuous measurement of extracellular H_2O_2 by this optical sensor with high sensitivity is a promising new means for real-time cytotoxicity tests, the investigation of oxidative stress and other physiological cell processes.

1. Introduction

Micropollutants (e.g. trace metals and inorganic nanoparticles) and abiotic factors (e.g. variations in temperature, salinity, UV irradiation) have been shown to negatively affect the cellular homeostasis of oxidants and antioxidants in aquatic microorganisms by enhancing the generation of reactive oxygen species (ROS) (Cap et al., 2012; Mallick and Mohn, 2000; Sies, 1986; von Moos et al., 2014; Xia et al., 2006). An overproduction of ROS can lead to the oxidative damage of subcellular components, including the membrane and DNA, and ultimately to cell death (Apel and Hirt, 2004; Maynard et al., 2006). Hydrogen peroxide (H_2O_2) is one of the most stable ROS, which can diffuse through the cell membrane (Dröge, 2002; Mallick and Mohn, 2000). Other ROS species are not likely to escape outside the cell due to their extremely short lifetimes: while micromolars of H_2O_2 decompose in about 12 h under normal conditions, $^1O_2$, $O_2^{\bullet -}$ and $OH^{\bullet}$ have lifetimes of 4 µs, 1 µs and 1 ns, respectively (Jin et al., 2010). Thus, tracing the kinetics of H_2O_2 in biological systems provides further insight into the mechanisms of oxidative stress (von Moos and Slaveykova, 2014).

ROS in biological systems are commonly detected using endpoint bioassays based on chemoluminescence and fluorescence (Chen et al., 2010, 2012; Jin et al., 2010; Miller et al., 2005). These methods, especially chemoluminescence, are very sensitive but continuous measurements are problematic because of their limited stability and deactivation by photobleaching (Kalyanaraman et al., 2012; Resch-Genger et al., 2008). Moreover, such probes can interfere with intracellular proteins and redox-cycling mechanisms (Kalyanaraman et al., 2012). Quantum dots (Qdots) are an interesting alternative to fluorescent labels thanks to their nanometer size and photostability (Gill et al., 2008; Resch-Genger et al., 2008). However, their limited biocompatibility is a drawback to their application in biological systems (Hoshino et al., 2004;

* Corresponding author.
E-mail address: christian.santschi@epfl.ch (C. Santschi).

http://dx.doi.org/10.1016/j.bios.2014.12.044
0956-5663/

Resch-Genger et al., 2008). The few available examples of real-time measurements mostly involve electrochemical biosensors (Suárez et al., 2013; Wightman, 2006). Yet, these suffer from electrode fouling, lack of long-run stability, and poor selectivity with respect to the analytes (Putzbach and Ronkainen, 2013). Alternatively, we have recently developed a novel optical tool for continuous measurements (Suarez et al., 2012, 2013). A difficulty associated with this approach lies in the fabrication of the sensing elements in a controlled and repeatable manner and the bulky nature of the optical setup.

Here, we present a portable oxidative stress sensor (POSS) for the non-invasive and continuous measurements of H_2O_2. This compact POSS was specifically designed for efficient and easy field analysis. We achieve a limit of detection (LOD) in the nanomolar range by tracing the optical response of spots with a few pmol of cyt *c*. Printing such spots in the porous substrate shows excellent repeatability and reproducibility and enhances their absorption thanks to multiscattering. During measurements, cyt *c* remains in the substrate and does not react directly with the living organisms present in the solution. This configuration has a non-invasive nature, enabling continuous measurements, which can be used to study the underlying dynamics. For calibration purposes, the kinetics of the biosensor response to different H_2O_2 concentrations is studied both in diffusion and flow regimes. For the latter case, we develop a reusable microfluidic device. Numerical simulations reveal no H_2O_2 depletion in the vicinity of the cyt *c* spot, indicating that diffusion effectively repletes H_2O_2 in the measurement chamber.

To demonstrate the potential use of the POSS in biological experiments, we study stress-related H_2O_2 release from the green microalga *C. reinhardtii*, a widespread microorganism present in soil and freshwater throughout the world. It is a primary producer at the base of the food chain and thus highly relevant from an ecotoxicological perspective (Grossman, 2007). To induce oxidative stress, algae were either treated with functionalized CdSe/ZnS core shell Qdots that are widely used as fluorescent labels (Dabbousi et al., 1997) or with TiO_2 nanoparticles, which are common constituents of everyday consumer products (Park et al., 2008). Elevated levels of H_2O_2 were successfully detected by means of the POSS. Hence, it is a promising new approach for the study of the mechanisms of oxidative stress in particular and of the interactions between nanomaterials and living organisms in general.

2. Materials and methods

2.1. Preparation of sensing spots

A microarray robot (QArray2, Genetix) was used to spot 4 mM aqueous cyt *c* (C2037, Sigma Aldrich) from a 384-well plate into the substrate – a filtration membrane (GSWP 220 nm, Millipore) – by a spotting pin (946MP8XB, Arrayit) with a delivery volume of 5 nl. Cyt *c* was partially crosslinked by exposing the freshly printed spots to glutaraldehyde (G5882, Sigma Aldrich) vapor for 1 h. The prepared samples were stored in water at 4 °C. To fully reduce the spots prior utilization, they were immersed into 1 ml of 10 μg/ml aqueous ascorbic acid (AA) solution for 30 min. The spots were subsequently washed 5 times for 10 min each in 1 ml distilled water.

2.2. Experimental design

For measurements in the static regime, a small chamber, delimited by an O-ring (9×1 mm^2, volume = 60 μl, No. 860110.0525, BRW), was filled with the solution of interest and the membrane containing the printed spot (Fig. 1a). The chamber was sealed with a cover slip and any excess liquid was removed. For every measurement a new O-ring and a new spot were used.

In the flow regime, the sensor spots were integrated into a microfluidic channel (0.3×1 mm^2 cross-section area and 4 mm length) fabricated in PDMS by molds prepared using standard photolithography (Fig. 1b). To guarantee an optimal tightness of the microfluidic channels, an additional PDMS layer (100 μm thickness) containing a hole to accommodate the porous membrane was added. These two PDMS layers along with the glass substrate were then clamped between two metallic plates. In order to optimize the performance of the sensor, the spot was aligned with respect to the center axis of the channel.

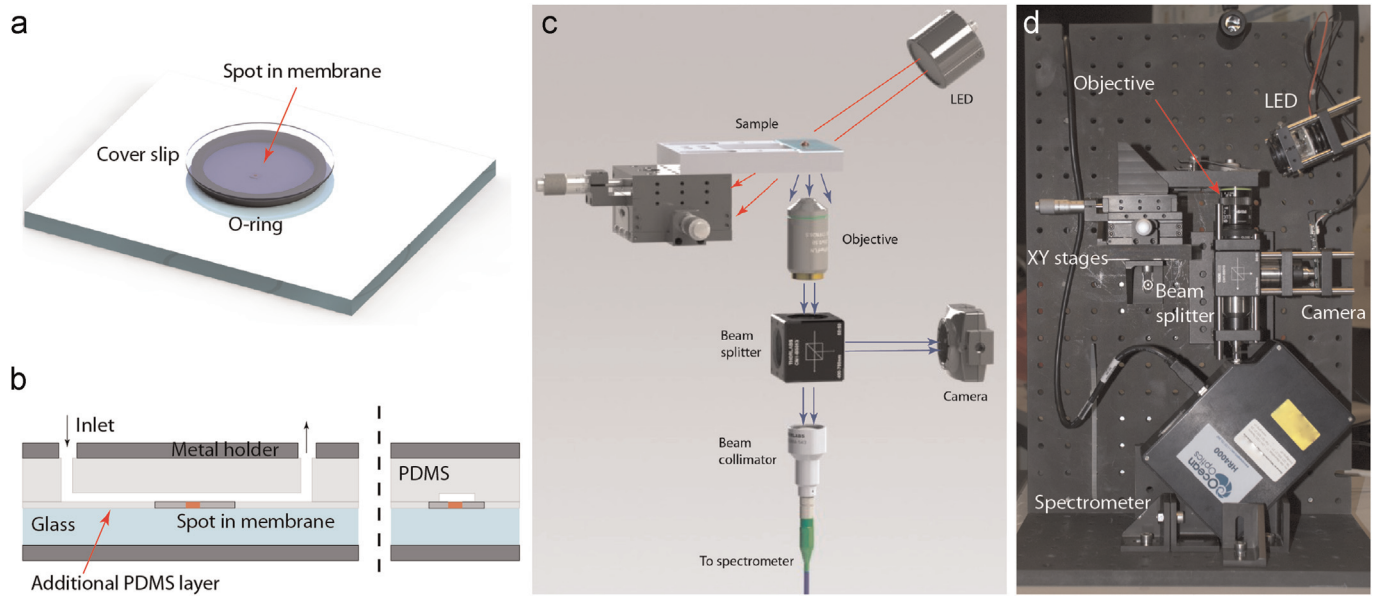

Fig. 1. Setup of the POSS. (a) Schematic illustration of the static regime configuration: the membrane containing the spot is placed onto the glass substrate in the O-ring. (b) Schematic illustration of the microfluidic configuration in the flow regime (side and front views). (c) Schematic drawing of the portable setup. For the sake of clarity, only the main elements are shown. Red arrows represent the light from the LED whereas blue arrows indicate the light scattered by the sample. (d) Picture of the portable setup (front view). (For interpretation of the references to color in this figure legend, the reader is referred to the web version of this article.)

The membranes were cut larger than the channels and were henceforth pinched by the top PDMS layer. Prior to the measurement, the channel was washed with PBS for 10 min at a constant flow of 2 mm/s. The solution of interest was then introduced at a constant flow rate (2 mm/s). At the end of every measurement, the spot was removed and all microfluidic components were thoroughly rinsed with distilled water. A new spot was then inserted for the next measurement. All measurements were performed in distilled water if not stated otherwise.

2.3. Optical measurements

All optical measurements were performed in transmission mode with the home-built POSS, where both systems – the static one and the microfluidic one – can be introduced. In order to guarantee a proper alignment and good stability, all components were fixed on a vertical mounting plate (Koman et al., 2013). The sample holder and all optical elements including the spectrometer and light source are situated on the front side of the mounting plate (Fig. 1c, d), whereas the electromechanical components, including the power supply (TXH 120 124, Traco Power) and liquid pump (Xcalibur, Tecan), were mounted on the rear side. The sample was fixed on an x–y-translation stage (Thorlabs, MT1/M), which allowed for proper alignment with the objective. A LED (R11/D3/N/B, Relco Group Ltd, 3W) was used as light source and the scattered light, containing the spectral information from the sample, was collected by the objective (UPlanFL 20x, Olympus, NA=0.45). The collimated beam at the output of the objective was split into a camera (C270, Logitech) for imaging the sample and a spectrometer (HR4000+, Ocean Optics) for spectral analysis of the scattered light. The objective was mounted on a z-translation stage in order to adjust the focal distance to the sample. Finally, the microfluidic pump was controlled with Labview. The entire portable setup has the dimensions $30 \times 15 \times 45$ cm^3.

2.4. Algal culture

The green alga *Chlamydomonas reinhardtii* strain (CPCC 11) was provided by the Canadian Phycological Culture Center. Axenic cultures were grown in four times diluted Tris–Acetate–Phosphate (TAP × 4) liquid medium and maintained in an incubator (Infors, Bottmingen, Switzerland) at 20 °C with a 24 h illumination regime (114.2 μmol phot/(m^2 s)) and constant rotary shaking (100 rpm). The algal culture was grown to a density of ca. 10^6 cells/ml.

2.5. Algal exposure

In order to transfer the algae from the growth medium to PBS, they were centrifuged at 3000 rpm for 5 min and the supernatant was replaced by the same amount of PBS. This procedure was repeated twice. For oxidative stress studies algae were mixed (1:1 in volume) either with 18 nm primary size TiO_2 nanoparticles (14021, Sigma), or cadmium ion solution (20893, Sigma) or CdSe/ZnS Qdots (Q21321MP, Life Technologies). To quench H_2O_2 in the measurement chamber, 100 μM of horseradish peroxidase (77332, Sigma Aldrich) was added to the sample 10 min prior to the measurement. To measure intracellular ROS, the sample was incubated with 20 μM CM-H_2DCFDA dye (Sigma Aldrich) for 30 min in the dark. Its fluorescent intensity was measured in a multi-well plate reader (Safire2, Tecan) at $\lambda=525$ nm with an excitation of $\lambda=495$ nm. Positive controls were obtained by exposing algae for 30 min to 10 mM H_2O_2 before subsequent incubation with CM-H_2DCFDA. To determine H_2O_2 concentrations, we also used an alternative end-point method: 250 μl of the sample was incubated with 25 μl of bioassay (STA-343, Cell Biolabs) for 30 min in the dark. Its absorption was measured in a multi-well plate reader at $\lambda=595$ nm and compared to the calibration curve made with H_2O_2 standards.

3. Detection principle and characterization

The core of the POSS consists of the hemoprotein cyt *c* whose spectral response reflects its average oxidation state (Kurihara and Sano, 1970; Margoliash and Frohwirt, 1959). In its reduced state cyt *c* exhibits a dip in the transmission spectrum at a wavelength $\lambda=550$ nm, which evolves into a broad small dip at $\lambda=530$ nm upon oxidation (Fig. 2b). Cyt *c* is oxidized in the presence of H_2O_2, which is simultaneously reduced to water. By monitoring the oxidation state of cyt *c* we can therefore trace the concentration of H_2O_2 present in the system. To quantify the oxidation state, we introduce a normalized oxidation state coefficient φ:

$$\varphi = \frac{A_{550}/A_{542} - A^{ox}_{550}/A^{*}_{542}}{A^{red}_{550}/A^{*}_{542} - A^{ox}_{550}/A^{*}_{542}}, \quad (1)$$

where A_{550} and A_{542} are the measured cyt *c* absorbance at $\lambda=550$ and $\lambda=542$ nm, respectively. A^{ox}_{550}, A^{red}_{550} and A^{*}_{542} are values taken from the literature, representing the absorbance for the oxidized and reduced states at $\lambda=550$ nm, and the absorbance at $\lambda=542$ nm, respectively (Butt and Keilin, 1962). The absorbance is calculated as follows: $A = -\log(I/I_0)$, where I and I_0 are the intensities measured after the light passed through the membrane with and without cyt *c*, respectively. The optical path length can vary between different measurements, which can lead to ambiguity if we would only normalize A_{550} between A^{ox}_{550} and A^{red}_{550}. To overcome this difficulty, we rather work with the ratio A_{550}/A_{542}, since the absorbance at $\lambda=542$ nm is independent of the oxidation state. In this way, the path length is canceled out as shown below. Taking into account Beer–Lambert's law ($A = \alpha C l$), Eq. (1) can be rewritten as follows:

$$\varphi = \frac{\alpha_{550}C_1l_1/\alpha_{542}C_1l_1 - \alpha^{ox}_{550}C_2l_2/\alpha^{*}_{542}C_2l_2}{\alpha^{red}_{550}C_2l_2/\alpha^{*}_{542}C_2l_2 - \alpha^{ox}_{550}C_2l_2/\alpha^{*}_{542}C_2l_2} = \frac{\alpha_{550} - \alpha^{ox}_{550}}{\alpha^{red}_{550} - \alpha^{ox}_{550}}, \quad (2)$$

where α_{550}, α_{542}, α^{ox}_{550}, α^{red}_{550} and α^{*}_{542} are the respective absorption coefficients. C_1 and l_1 are the cyt *c* concentration and the optical length through the sample and C_2 and l_2 the respective values from the literature (Butt and Keilin, 1962). This normalization results in $\varphi=1$ for the fully reduced and $\varphi=0$ for the fully oxidized state of cyt *c*.

So far, Vandewalle and Petersen (1987) detected micromolars of H_2O_2 by measuring A_{550} of cyt *c* in solution. In order to detect lower H_2O_2 concentrations, the cyt *c* absorbance *A* must be amplified. Recently, we have proposed a multiscattering approach where cyt *c* is embedded in a highly scattering medium composed of polystyrene beads, leading to an enhanced *A* (Suarez et al., 2013). This configuration showed insufficient repeatability and reproducibility, since each polystyrene beads aggregate is different. Here we present an elegant and fast approach to achieve a reproducible multiscattering configuration: picomole drops of cyt *c* are printed in a filter membrane using a fully automated liquid dispenser (Fig. 2a). This procedure yields spots with diameters of 0.6 mm and 2 mm for membranes with pore sizes of 220 nm and 450 nm, respectively.

Optical measurements show an increased absorption of cyt *c* in the membrane compared to the same amount of cyt *c* deposited on a flat glass substrate (Fig. 2c). This effect is caused by two factors: (1) due to the surface tension, drops on the glass surface form a thin layer (<10 μm), resulting in a smaller optical thickness; (2) light scattering taking place in the pores of the membrane enhances the optical path length (Svensson et al., 2011). The enhancement factor f is defined as the ratio between cyt *c*

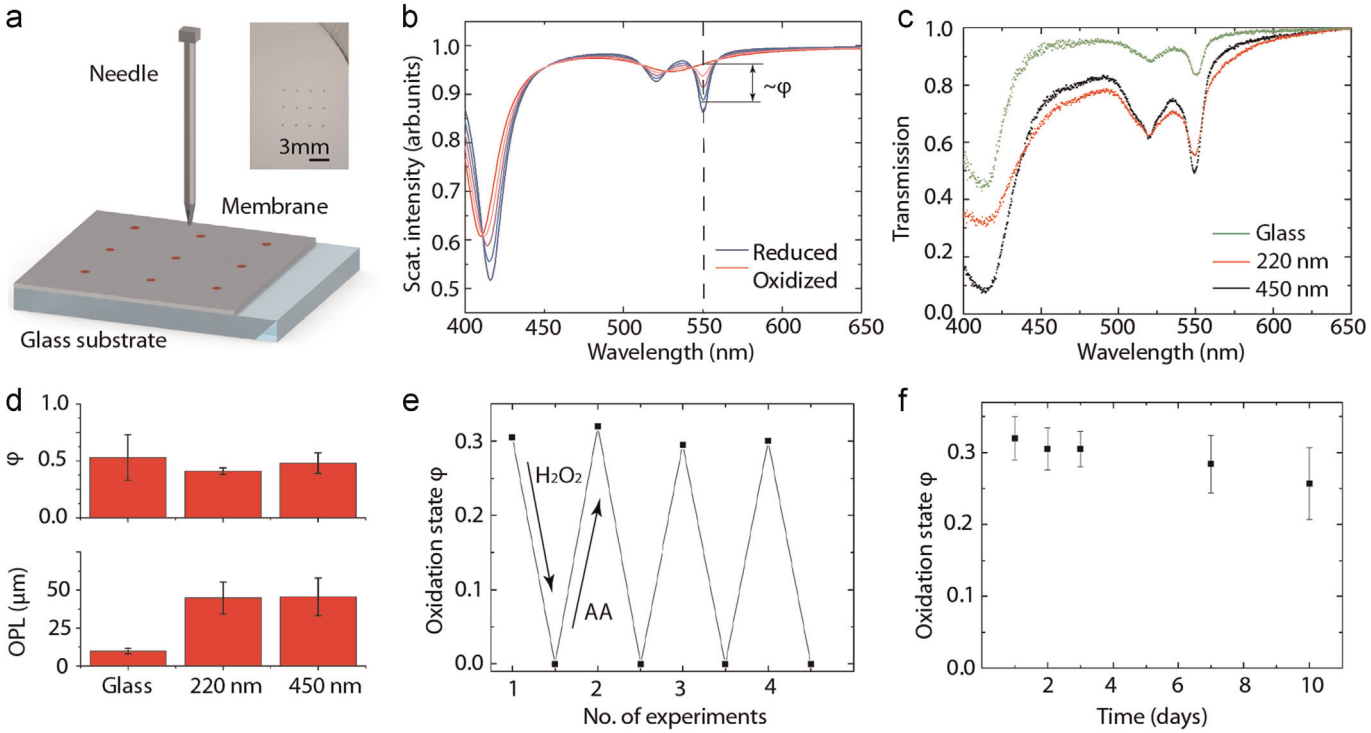

Fig. 2. Printed cyt *c* spots. (a) Schematic illustration of contact printing of cyt *c* onto the membrane. The inset shows a photograph of an array of printed spots. (b) Spectral response of cyt *c* from reduced to oxidized states. (c) Optical transmission of 20 pmol cyt *c* spots printed on glass, in 220 nm, or in 450 nm pore size membranes in the presence of AA. (d) Oxidation state φ in the presence of AA and the optical path length (OPL) for spots on glass, in 220 nm and 450 nm pore membranes. The error bars correspond to the standard deviation of 9 measurements. (e) Oxidation state φ of a cyt *c* spot in a 220 nm pore size membrane in AA and H_2O_2 as a function of the number of consecutive oxidation/reduction cycles (calculated using Eq. (1)). Prior to their utilization, the spots were reduced with AA and subsequently washed as described in Section 2. The washing process decreased the initial φ with respect to the values in (d). φ was measured immediately after the addition of 20 μM of H_2O_2 and 30 min later. (f) Oxidation state φ of a cyt *c* spot in a 220 nm pore size membrane as a function of storage time. The spots were prepared as in (e). The error bars represent the standard deviation for 5 measurements.

absorbance A at $\lambda = 542$ nm for a spot on glass and a spot in the membrane. For a 20 pmol spot f is 4.6 ± 0.8 and 4.6 ± 1.2 in membranes with pore sizes 220 nm and 450 nm, respectively (Fig. 2d). Due to crosslinking, cyt *c* is partially denatured, remaining in its oxidized form and loses some of its pseudo-peroxidase behavior, which is essential for our sensing purpose. To estimate the degree of denaturation, we measured the spectral response of several spots which were reduced in excess of AA (Fig. 2c, d). Spots deposited on glass and in 220 nm and 450 nm pore size membranes show φ values of 0.53 ± 0.20, 0.41 ± 0.03 and 0.48 ± 0.09.

Cyt *c* in solution can be reversibly oxidized and reduced (Margoliash and Frohwirt, 1959). Similarly, a completely oxidized spot can be reduced to its original oxidation state and hence, re-used for H_2O_2 detection up to five times (Fig. 2e). However, high H_2O_2 concentrations (> 100 μM) irreversibly oxidize and denature cyt *c* (Margoliash and Frohwirt, 1959). Yet, ten days old spots have constant coefficients φ demonstrating a good lifetime for the sensing element (Fig. 2f).

4. Calibration and modeling

In order to relate the oxidation state φ to the H_2O_2

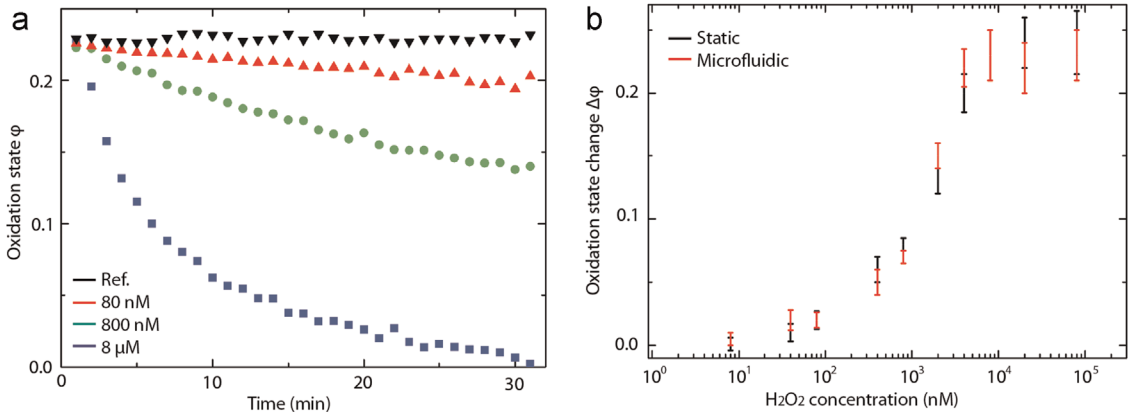

Fig. 3. Kinetics of cyt *c* oxidation in the presence of H_2O_2. (a) Time evolution of the oxidation state φ for different H_2O_2 concentrations for a 20 pmol spot of cyt *c* in a 220 nm pore membrane in the static regime (calculated using Eq. (1)). The reference measurements are performed in distilled water. (b) Calibration curve of the change of the oxidation state $\Delta\varphi$ after 30 min for the static and microfluidic regimes. Error bars represent the standard deviation over 3 measurements.

concentration, calibration experiments were performed. The kinetics of φ at different H_2O_2 concentrations in the static regime is shown in Fig. 3a. While 80 nM H_2O_2 only slightly oxidizes cyt *c* ($\Delta\varphi = \varphi_0 - \varphi_t = 0.02$), 8 μM leads to a complete oxidation within 30 min. φ_0 and φ_t represent the oxidation states at $t=0$ and $t=30$ min, respectively. In the absence of H_2O_2 there is a slow oxidation of cyt *c* ($\Delta\varphi$ around 0.005 per 30 min) which has to be taken into account for data analysis. The calibration curve resembles a sigmoidal shape typical of such reactions (Fig. 3b). The LOD, defined as the 3-fold of standard deviation, is 40 nM. For comparison, recently reported schemes for continuous H_2O_2 detection – based on fluorescent carbon nanotubes and electrochemistry – have their LODs in the micromolar (Jin et al., 2010; Kim et al., 2013). The upper detection limit of the sensor corresponds to 4 μM for a 30 min measurement. Even higher H_2O_2 concentrations can be measured by tracking φ for shorter time periods. For a time interval of 1 min, we estimate an upper detection limit of 80 μM for a 20 pmol cyt *c* spot. Finally, a calibration curve in PBS matches with that in distilled water (data not shown).

As follows from Fig. 2d, roughly 40% of the cyt *c* – corresponding to 8 pmol – remains active after crosslinking. On the other hand, the 60 μl O-ring filled with 80 nM H_2O_2 corresponds to 4.8 pmol. Provided a 1:1 stoichiometric relation, H_2O_2 can maximally oxidize 60% of cyt *c* in the spot. However, the reaction is very slow and within 30 min we only observe 2% oxidation. This can be due to the depletion of H_2O_2 near the cyt *c* spot and/or to slow reaction kinetics. Since a similar behavior is observed in both static and microfluidic regimes, we exclude the H_2O_2 depletion scenario. Below, we provide a more quantitative discussion of the reaction kinetics.

The reaction between cyt *c* and H_2O_2 is described by Fenton's reaction (Haber and Weiss, 1932):

$$Fe^{2+} + H_2O_2 = Fe^{3+} + HO\bullet + OH^- \quad (3)$$

The rate of reaction (3) is only determined by the availability of H_2O_2 and cyt *c* and can be expressed as follows:

$$\begin{cases} \dfrac{dN_{H2O2}}{dt} = -\tilde{k} N_{H2O2} N_{cytc} \\ \dfrac{dN_{cytc}}{dt} = \dfrac{dN_{H2O2}}{dt} \end{cases}, \quad (4)$$

where N_{cytc} and N_{H2O2} stand for the number of molecules of reduced cyt *c* and H_2O_2, respectively; $\tilde{k}$ is the reaction constant. In the microfluidic case fresh H_2O_2 is continuously injected into the system, resulting in a constant H_2O_2 concentration. Consequently, a first order approximation which fulfills Eq. (3) can be applied:

$$N_{cytc} = N^0_{cytc} e^{-N_{H2O2}\tilde{k}t}, \quad (5)$$

where N^0_{cytc} is the reduced amount of cyt *c* at $t=0$. Dividing Eq. (4) by the total amount of cyt *c* and introducing $k = \tilde{k}V$ (V is the volume of the chamber) results in

$$\varphi = e^{-C_{H2O2}kt}. \quad (6)$$

The interaction constant k is obtained by fitting Eq. (6) to the experimental data (Fig. 3a), yielding 0.24 ± 0.06 min^{-1} μM^{-1}. The obtained values agree well with data from literature for the interaction between cyt *c* and H_2O_2 in solution (0.13 min^{-1} μM^{-1}) (Vandewalle and Petersen, 1987).

We propose a 1D diffusion model with a cyt *c* layer at $x=0$ to simulate the reaction kinetics and the diffusion of H_2O_2 in the static configuration (Fig. 4a). The kinetics of the cyt *c* – H_2O_2 reaction is described by Eq. (4) and the reaction itself takes place in the proximity of the cyt *c* spot. H_2O_2 diffusion is simulated with the diffusion constant $D=10^{-9}$ m^2/s (Gregory and Clary, 1995). We study the reaction kinetics using two extreme conditions: (1) $N^0_{H2O2} \gg N^0_{cytc}$ and (2) $N^0_{H2O2} \ll N^0_{cytc}$, and compare them with the microfluidic regime, where N^0_{H2O2} is constant over time. In the first case, we consider $N^0_{cytc}=20$ pmol of fully reduced cyt *c* and $N^0_{H2O2}=480$ pmol H_2O_2 (equivalent to $C_{H2O2}=8$ μM in the reaction chamber). Only 2% of C_{H2O2} is sufficient to fully oxidize cyt *c* within 30 min (Fig. 4b,c). Static and microfluidic responses are identical, which is in agreement with our experiments. In the second case, we analyze $N^0_{cytc}=20$ pmol cyt *c* and $N^0_{H2O2}=0.48$ pmol H_2O_2

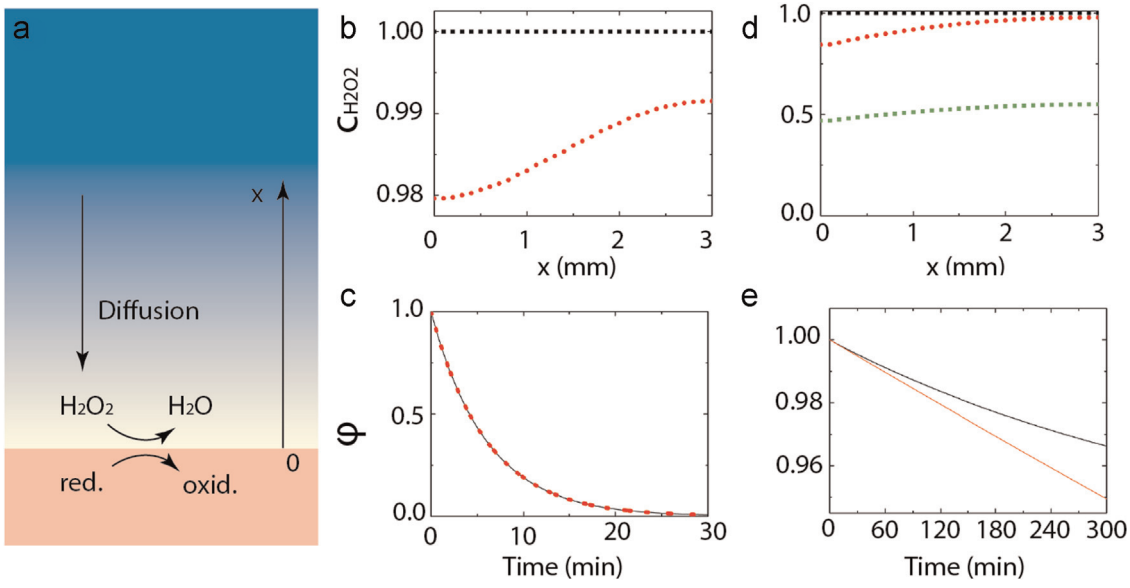

Fig. 4. Biosensor response simulations. (a) Schematic of the 1D simulation showing a chamber filled with H_2O_2 reacting with cyt *c* at the interface $x=0$. (b) Normalized H_2O_2 concentration C_{H2O2} for 20 pmol cyt *c* and 480 pmol H_2O_2 at $t=0$ (black) and 30 min (red). (c) Oxidation state φ kinetics for the reaction in (b) for the microfluidic (dotted red) and static (black, overlaps) regimes. (d) C_{H2O2} for 20 pmol cyt *c* and 0.48 pmol H_2O_2 interaction at $t=0$ (black), 30 min (red) and 5 h (green). (e) Oxidation state φ kinetics for the reaction in (d) for the microfluidic (red) and static (black) regimes. (For interpretation of the references to colour in this figure legend, the reader is referred to the web version of this article.)

(equivalent to $C_{H2O2}=8$ nM). Even after 5 h no H_2O_2 depletion occurs (Fig. 4d). φ changes slowly from 1 to 0.97 (Fig. 4e). The difference between static and microfluidic regimes becomes significant only after 3 h, due to the H_2O_2 consumption in the former, while for shorter periods the φ responses are the same. Thus, our simulations confirm similar reaction kinetics in both regimes. Eqs. (5) and (6) can therefore be extended to the static case. Also, the presence of the cyt *c* spot only slightly affects the H_2O_2 concentration and, consequently, does not deteriorate the measurements.

In biological systems H_2O_2 is generated with time-dependent rates. We can quantify the H_2O_2 concentration at a given time *t* with Eq. (5) by considering the derivative of the measured φ value:

$$\frac{d\varphi/dt}{\varphi} = \frac{dN_{cytc}/dt}{N_{cytc}} = -kC_{H2O2}. \tag{7}$$

Finally, we introduce the probability of cyt *c* to be oxidized in the presence of a given H_2O_2 concentration. This coefficient is defined as the ratio between the amount of H_2O_2 that interacts with cyt *c* ($dN_{interact}$) and the amount that reaches the spot in a given second (dN_0). The first quantity can be calculated using Eq. (7), while the latter is obtained from the molecular dynamics theory as the number of molecules hitting the surface in a given time:

$$\begin{aligned}\psi &= \left|\frac{dN_{interact}}{dN_0}\right| \\ &= \left|\frac{dN_{H2O2}/dt}{1/4(C_{H2O2}v_{H2O2}A_{spot})}\right| \\ &= \frac{kC_{H2O2}N_{cytc}}{1/4(C_{H2O2}v_{H2O2}A_{spot})} \\ &= 4\frac{\varphi k N^0_{cytc}}{3D/l_{free}(A_{spot})} \\ &= \frac{4kN^0_{cytc}l_{free}}{3DA_{spot}}\varphi,\end{aligned} \tag{8}$$

where v_{H2O2} is the thermal velocity of H_2O_2 molecule in water, A_{spot} the area of the sensing spot ($\approx 2.83\times10^{-7}$ m^2), l_{free} the mean free path of H_2O_2 molecules in water ($\approx$0.25 nm). ψ does not depend on the H_2O_2 amount and is only a property of the cyt *c* spot. A given spot can be fully characterized by N^0_{cytc} and A_{spot}, by introducing the unitless coefficient of interaction:

$$\gamma = k\frac{4N^0_{cytc}l_{free}}{3DA_{spot}}. \tag{9}$$

It can be approximated by $\gamma \approx 9.4\times10^{-5}$, representing the probability of H_2O_2 to oxidize cyt *c* when reaching the fully reduced spot surface ($\varphi = 1$). Finally, with $\psi = \gamma\varphi$, the probability of interaction with cyt *c* decreases proportionally with φ.

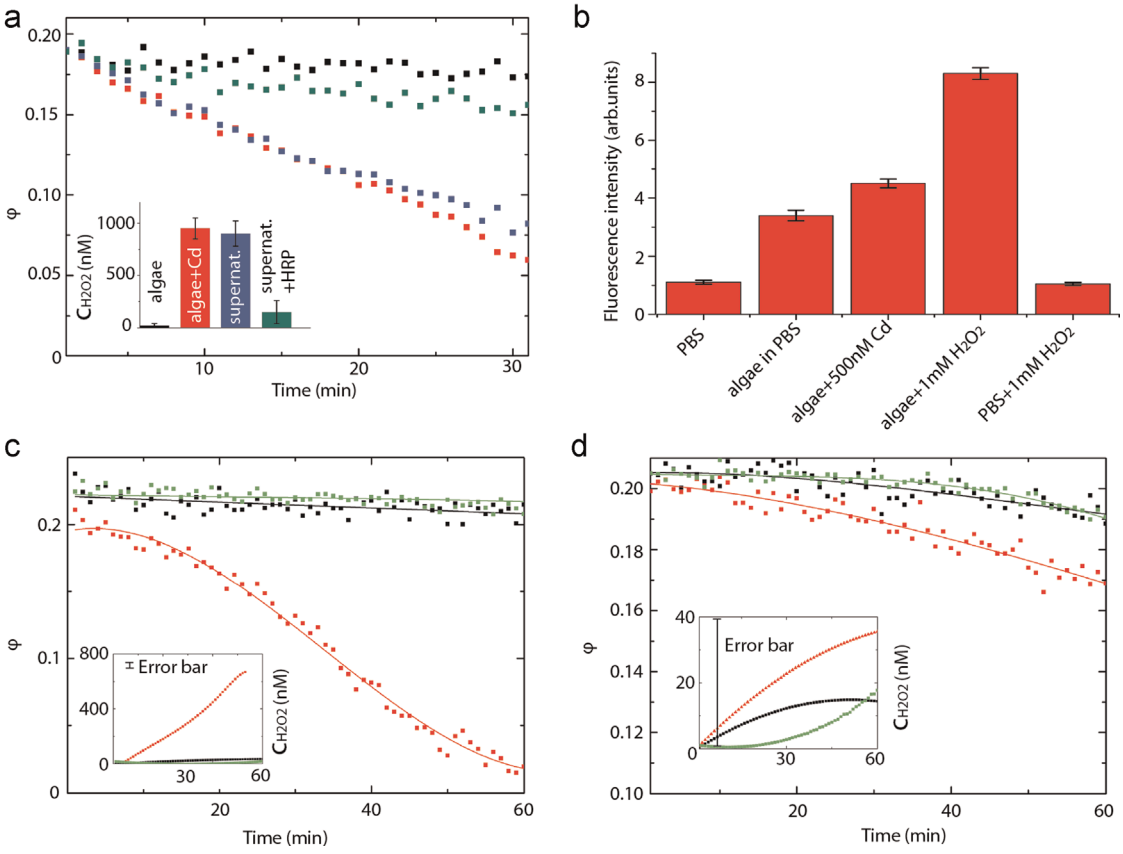

Fig. 5. (a) Time evolution of φ for algae (black), algae incubated in 500 nM Cd for 2 h (red), supernatant extracted from it (dark blue) and a mixture of supernatant with 100 μM HRP (green). The corresponding inset shows the time average C_{H2O2} calculated using Eq. (7) (C_{H2O2} does not change significantly with time). (b) Intracellular ROS fluorescence intensity of 20 μM CM-H_2DCFDA dye. Error bars represent the standard deviation over 3 measurements. Time evolution of φ for algae suspended in PBS solution (black) and algae exposed to (c) 140 nM of CdSe/ZnS Qdots and (d) 10 mg/l TiO_2 nanoparticles (red). Respective control curves of only Qdots and nanoparticles are shown in green. All curves are fitted with a polynomial function. Insets show the time evolution of C_{H2O2} calculated using Eq. (7). (For interpretation of the references to colour in this figure legend, the reader is referred to the web version of this article.)

5. Applications

To demonstrate the performance of the POSS, we study the kinetics of stress-related H_2O_2 released by *C. reinhardtii* in the static configuration. First, algae were exposed to 500 nM Cd(II), which is highly toxic and known to induce oxidative stress in algae (Suarez et al., 2013). Indeed, after 2 h of exposure, we measured a H_2O_2 concentration of $C_{H2O2} = 950 \pm 100$ nM in the Cd/algae suspension (Fig. 5a). Unexposed algae do not produce any H_2O_2 with the respective C_{H2O2} values being below the detection limit. Intracellular ROS levels increase in identical conditions, correlating well with our findings (Fig. 5b). To exclude a possible interference of cells, Cd or ROS with the sensing element, we carefully extracted the supernatant from the sample by centrifugation. The obtained C_{H2O2} values of the supernatant (900 ± 120 nM) are in excellent agreement with that in the Cd/algae suspension. Moreover, an alternative end-point bioassay confirmed the presence of H_2O_2 in the supernatant with $C_{H2O2} = (1.0 \pm 0.3\ \mu M)$. To further demonstrate that POSS indeed senses H_2O_2, we added 100 µM horseradish peroxidase (HRP) to the supernatant to selectively catalyze the decomposition of H_2O_2 into water. As a result, C_{H2O2} decreased to the background values of the negative controls (130 ± 110 nM).

Next, we expose algae to 140 nM Qdots (Fig. 5c) and 10 mg/l TiO_2 nanoparticles (Fig. 5d). Qdots induce a rapid increase of C_{H2O2} already after 5 min that reaches a value of 700 nM at 1 h. This indicates the oxidative stress, which was also observed for the same Qdots in smaller concentrations but for longer exposure times (Kirchner et al., 2004). On the other hand, algae exposed to 10 mg/l TiO_2 nanoparticles produced 40 nM H_2O_2 after 1 h, proving that TiO_2 nanoparticles do not induce elevated ROS levels in algae at this concentration (Clément et al., 2013). Control experiments with Qdots/nanoparticles suspended in PBS without algae did not show any effect on the oxidation state of cyt *c*.

6. Conclusions

In this paper we have presented a new portable device for the continuous measurement of the kinetics of oxidative stress. By printing 20 pmol cyt *c* spots in a porous membrane containing 220 nm pores, the optical absorbance of cyt *c* is increased by a factor of 4.6 thanks to the elongation of the optical path. This configuration reaches a LOD of 40 nM. The spots can be stored up to 10 days without losing their functionality. Moreover, they can be re-reduced and reused for at least 5 measurements. The POSS is easy to handle and shows a high reproducibility, which makes it a very well suited tool for the detection of H_2O_2 in the context of a broad variety of biological systems. Experimental results and numerical simulations show that the diffusion rate of H_2O_2 is faster than the chemical reaction rate between cyt *c* and H_2O_2. Additionally, by careful consideration on the reaction kinetics, we have derived an expression allowing the determination of H_2O_2 for time-dependent biological processes, which validity we demonstrated exemplarily by exposing *C. reinhardtii* cells to 180 nM Qdots and to 50 mg/l TiO_2 nanoparticles. Oxidative stress occurred in Qdots with continuously increasing H_2O_2 release (14 nM/min), starting after 5 min of exposure, while this was not observed in the case of TiO_2. Hence, POSS has the potential to shine new light on specific environmental questions in the field as well as in the laboratory (Maynard et al., 2006).

Acknowledgment

This work was supported by the Swiss National Research Program NRP 64 project no. 406440-131280/1 of the Swiss National Science Foundation. We are very grateful to Prof. Sebastian Maerkl for the utilization of the microarray robot.

References

Apel, K., Hirt, H., 2004. Reactive oxygen species: metabolism, oxidative stress, and signal transduction. Annu. Rev. Plant Biol. 55 (1), 373–399.
Butt, W.D., Keilin, D., 1962. Absorption spectra and some other properties of cytochrome c and of its compounds with ligands. Proc. R. Soc. Lond. Ser. B, Biol. Sci. 156 (965), 429–458.
Cap, M., Libuse, V., Palková, Z., 2012. Reactive oxygen species in the signaling and adaptation of multicellular microbial communities. Oxid. Med. Cell. Longev. 2012, 13.
Chen, H., Li, R., Lin, L., Guo, G., Lin, J.-M., 2010. Determination of l-ascorbic acid in human serum by chemiluminescence based on hydrogen peroxide–sodium hydrogen carbonate–CdSe/CdS quantum dots system. Talanta 81 (4–5), 1688–1696.
Chen, W., Hong, L., Liu, A.-L., Liu, J.-Q., Lin, X.-H., Xia, X.-H., 2012. Enhanced chemiluminescence of the luminol-hydrogen peroxide system by colloidal cupric oxide nanoparticles as peroxidase mimic. Talanta 99 (0), 643–648.
Clément, L., Hurel, C., Marmier, N., 2013. Toxicity of TiO_2 nanoparticles to cladocerans, algae, rotifers and plants – effects of size and crystalline structure. Chemosphere 90 (3), 1083–1090.
Dabbousi, B.O., Rodriguez-Viejo, J., Mikulec, F.V., Heine, J.R., Mattoussi, H., Ober, R., Jensen, K.F., Bawendi, M.G., 1997. (CdSe)ZnS core – shell quantum dots: synthesis and characterization of a size series of highly luminescent nanocrystallites. J. Phys. Chem. B 101 (46), 9463–9475.
Dröge, W., 2002. Free radicals in the physiological control of cell function. Physiol. Rev. 82 (1), 47–95.
Gill, R., Bahshi, L., Freeman, R., Willner, I., 2008. Optical detection of glucose and acetylcholine esterase inhibitors by H_2O_2-sensitive CdSe/ZnS quantum dots. Angew. Chem. 120 (9), 1700–1703.
Gregory, J.K., Clary, D.C., 1995. Calculations of the tunneling splittings in water dimer and trimer using diffusion Monte Carlo. J. Chem. Phys. 102 (20), 7817–7829.
Grossman, A., 2007. In the grip of algal genomics. In: León, R., Galván, A., Fernández, E. (Eds.), Transgenic Microalgae as Green Cell Factories. Springer, New York, pp. 54–76.
Haber, F., Weiss, J., 1932. Über die Katalyse des Hydroperoxydes. Naturwissenschaften 20 (51), 948–950.
Hoshino, A., Fujioka, K., Oku, T., Suga, M., Sasaki, Y.F., Ohta, T., Yasuhara, M., Suzuki, K., Yamamoto, K., 2004. Physicochemical properties and cellular toxicity of nanocrystal quantum dots depend on their surface modification. Nano Lett. 4 (11), 2163–2169.
Jin, H., Heller, D.A., Kalbacova, M., Kim, J.-H., Zhang, J., Boghossian, A.A., Maheshri, N., Strano, M.S., 2010. Detection of single-molecule H_2O_2 signalling from epidermal growth factor receptor using fluorescent single-walled carbon nanotubes. Nat. Nano 5 (4), 302–309.
Kalyanaraman, B., Darley-Usmar, V., Davies, K.J.A., Dennery, P.A., Forman, H.J., Grisham, M.B., Mann, G.E., Moore, K., Roberts, Ii, L.J., Ischiropoulos, H., 2012. Measuring reactive oxygen and nitrogen species with fluorescent probes: challenges and limitations. Free Radic. Biol. Med. 52 (1), 1–6.
Kim, G., Lee, Y.-E., Kopelman, R., 2013. Hydrogen peroxide (H_2O_2) detection with nanoprobes for biological applications: a mini-review. In: Armstrong, D., Bharali, D.J. (Eds.), Oxidative Stress and Nanotechnology. Springer Science +Business Media, New York, pp. 101–114.
Kirchner, C., Liedl, T., Kudera, S., Pellegrino, T., Muñoz Javier, A., Gaub, H.E., Stölzle, S., Fertig, N., Parak, W.J., 2004. Cytotoxicity of colloidal CdSe and CdSe/ZnS nanoparticles. Nano Lett. 5 (2), 331–338.
Koman, V., Suárez, G., Santschi, C., Cadarso, V.J., Brugger, J., von Moos, N., Slaveykova, V.I., Martin, O.J.F., 2013. A portable microfluidic-based biophotonic sensor for extracellular H_2O_2 measurements. Proc. SPIE, 857218-1–857218-7.
Kurihara, M., Sano, S., 1970. Reduction of cytochrome c by ferrous ions and ethylenediaminetetraacetic acid in acid solution. J. Biol. Chem. 245 (18), 4804–4806.
Mallick, N., Mohn, F.H., 2000. Reactive oxygen species: response of algal cells. J. Plant Physiol. 157 (2), 183–193.
Margoliash, E., Frohwirt, N., 1959. Spectrum of horse-heart cytochrome c. Biochem. J. 71 (1), 570–572.
Maynard, A.D., Aitken, R.J., Butz, T., Colvin, V., Donaldson, K., Oberdorster, G., Philbert, M.A., Ryan, J., Seaton, A., Stone, V., Tinkle, S.S., Tran, L., Walker, N.J., Warheit, D.B., 2006. Safe handling of nanotechnology. Nature 444 (7117), 267–269.
Miller, E., Albers, A., Pralle, A., Isacoff, E., Chang, C., 2005. Boronate-based fluorescent probes for imaging cellular hydrogen peroxide. J. Am. Chem. Soc. 127 (47), 16652–16659.
Park, E.-J., Yi, J., Chung, K.-H., Ryu, D.-Y., Choi, J., Park, K., 2008. Oxidative stress and apoptosis induced by titanium dioxide nanoparticles in cultured BEAS-2B cells. Toxicol. Lett. 180 (3), 222–229.
Putzbach, W., Ronkainen, N., 2013. Immobilization techniques in the fabrication of nanomaterial-based electrochemical biosensors: a review. Sensors 13 (4), 4811–4840.
Resch-Genger, U., Grabolle, M., Cavaliere-Jaricot, S., Nitschke, R., Nann, T., 2008. Quantum dots versus organic dyes as fluorescent labels. Nat. Methods 5 (9),

763–775.
Sies, H., 1986. Biochemistry of oxidative stress. Angew. Chem. Int. Ed. Engl. 25 (12), 1058–1071.
Suarez, G., Santschi, C., Dutta-Gupta, S., Juillerat-Jeanneret, L., Martin, O.J.F., 2012. Biophotonic tool for sensing the dynamics of H_2O_2 extracellular release in stressed cells. Proc. SPIE 8229, 822908-1–822908-7.
Suárez, G., Santschi, C., Martin, O.J.F., Slaveykova, V.I., 2013. Biosensor based on chemically-designed anchorable cytochrome c for the detection of H_2O_2 released by aquaticcells. Biosens. Bioelectron. 42 (0), 385–390.
Suarez, G., Santschi, C., Slaveykova, V.I., Martin, O.J.F., 2013. Sensing the dynamics of oxidative stress using enhanced absorption in protein-loaded random media. Sci. Rep. 3, 03447-1–03447-8.
Svensson, T., Adolfsson, E., Lewander, M., Xu, C.T., Svanberg, S., 2011. Disordered, strongly scattering porous materials as miniature multipass gas cells. Phys. Rev. Lett. 107 (14), 143901.
Vandewalle, P.L., Petersen, N.O., 1987. Oxidation of reduced cytochrome c by hydrogen peroxide. Implic. Superoxide Assays 210 (2), 195–198.
von Moos, N., Bowen, P., Slaveykova, V.I., 2014. Bioavailability of inorganic nanoparticles to planktonic bacteria and aquatic microalgae in freshwater. Environ. Sci.: Nano 1 (3), 214–232.
von Moos, N., Slaveykova, V.I., 2014. Oxidative stress induced by inorganic nanoparticles in bacteria and aquatic microalgae – state of the art and knowledge gaps. Nanotoxicology 8 (6), 605–630.
Wightman, R.M., 2006. Probing cellular chemistry in biological systems with microelectrodes. Science 311 (5767), 1570–1574.
Xia, T., Kovochich, M., Brant, J., Hotze, M., Sempf, J., Oberley, T., Sioutas, C., Yeh, J.I., Wiesner, M.R., Nel, A.E., 2006. Comparison of the abilities of ambient and manufactured nanoparticles to induce cellular toxicity according to an oxidative stress paradigm. Nano Lett. 6 (8), 1794–1807.